COMPUTER MODELLING OF INTERFACIAL TRANSITION ZONE: MICROSTRUCTURE AND PROPERTIES

by

Dale P. Bentz and Edward J. Garboczi
Building and Fire Research Laboratory
National Institute of Standards and Technology
Gaithersburg, MD 20899 USA

Reprinted from Engineering and Transport Properties of the Interfacial Transition Zone in Cementitious Composites, RILEM Report No. 20, RILEM Publications s.a.r.l., ENS – 61 Av Pdt Wilson, F-94235 Cachan Cedex, France, M. G. Alexander; G. Arliguie; G. Ballivy; A. Bentur and J. Marchand, Editors, Part 5, Chapter 20, pp 349-385, 1999.

NIST
National Institute of Standards and Technology
Technology Administration, U.S. Department of Commerce

COMPUTER MODELLING OF INTERFACIAL TRANSITION ZONE: MICROSTRUCTURE AND PROPERTIES

Prepared by Dale P. Bentz and Edward J. Garboczi
National Institute of Standards and Technology
Gaithersburg, Maryland USA

1. Introduction

Many of the experimental advances in understanding interfacial transition zone (ITZ) microstructure and its role in the performance of cement-based composites have been either initiated or accompanied by advances in the computer modelling of ITZ microstructure and properties. In the early stages of research in this area, conceptual models explaining ITZ formation and structure were proposed [1]. With the advances in computational capability in recent years, these conceptual models have been substantiated and further developed via computer simulations [2,3]. This chapter provides a review of the computational techniques that have been employed in these simulations and the results obtained, covering both ITZ formation and structure and the resulting effect on the properties of cement-based materials.

2. Continuum and Digital Image Microstructure Models

There are two general methods used to actually simulate microstructure in a computer. By simulate we mean that in some way, at any position in the space considered by the model, it is known what material phase, solid or porosity, exists at that point. These two methods are the *continuum* and *digital-image-based* methods. Both are used in the computer modelling of ITZ microstructure, and are complementary.

In a continuum model, one thinks of particles embedded in a matrix. Each solid particle is represented as a simple geometrical shape (such as a sphere or an ellipsoid) and is characterized by its centroid location, dimension, and orientation. For a sphere, this requires only the (x,y,z) coordinates of the sphere center and its radius. For an ellipsoid, in addition to the centroid coordinates, the lengths of the three semiaxes are required, along with three angles describing the orientation of the ellipsoid [4]. Particles following a representative particle size distribution are placed into a three-dimensional computational volume in a random configuration according to some placement statistics. A common way of placing particles is that the particles do not overlap. This covers the case of aggregates in concrete, or cement particles in water. To accomplish this kind of placement, particles to be placed must be checked for overlap with existing particles. If an overlap exists, the new particle is removed and placed randomly elsewhere. Checking for the overlap of two spherical particles, given their centroids and radii, is computationally trivial. The center of two particles may not come closer than the sum of their radii. Examining the overlap of two general ellipsoids is mathematically more challenging, but still tractable [4,5].

The major advantage of a continuum approach is that the memory requirement for representing a relatively large volume of material is small. For example, concretes containing on the order of one million aggregate particles have been simulated using this approach [6], since only four (for spheres) and nine (for tri-axial ellipsoids) million numbers need to be stored for this size system. This gives a total computer memory requirement of 32-72 MBytes (at eight bytes per number or about 16 significant figures), which is not a large amount of memory for modern computers.

In a digital-image-based model, the computational volume is subdivided into a three-dimensional array of individual cubic elements, typically called pixels or voxels. Here, each cement or aggregate particle can be composed of many pixels. In this way, complex shapes and phase distributions which defy simple geometric descriptions can be represented at finite resolution. When a complex random process like hydration is considered, with the microstructure undergoing re-distribution of material and the random growth of new phases, a digital-image-based method becomes absolutely necessary to capture what is happening in the microstructure.

For modelling cement paste, the resolution typically employed is on the order of 1 μm / pixel. After approximating the initial configuration of multi-size, multi-phase cement particles in water, cellular automata techniques are employed to simulate the hydration reactions and developing microstructure in three dimensions [7,8]. Rules which maintain the appropriate volume stoichiometry have been developed and implemented for the dissolution, diffusion, and reaction of the starting cement clinker phases as detailed in Refs. [7,8].

3. Computer Modelling of Interfacial Transition Zone Formation and Structure

The usual theoretical approach to analyzing the microstructure and properties of composite materials [9,10], where the matrix is a known quantity, is to first examine the dilute limit, where the inclusion phase is at a such a low volume fraction that each particle can be considered separately from all the others. One then builds up the full composite and examines the effect of having many inclusions. Later in this chapter a multi-scale approach to modelling the microstructure of concrete [11] will be studied, in which, analogous to the composite approach given above, one first develops models on different length scales and then links such models together to try to understand the full multi-scale problem. Consistent with this approach, the microstructure of the ITZ can be considered at two levels: the formation of microstructure near a single aggregate particle surface, and the formation of a global network of ITZ microstructure throughout the concrete.

3.1 Single Aggregate Models

The first object of study is the microstructure in the ITZ surrounding a single aggregate. The main interest lies in accurately portraying the characteristics of the cement particles and the mechanisms of ITZ microstructural development due to cement hydration. Before hydration occurs, a continuum model or a digital model can be used. Only a digital model, however, is effective in handling the random microstructural changes that occur during hydration.

3.1.1 Initial ITZ Microstructure

Continuum modelling has been used to study the effects of particle size distribution and water-to-cement (w/c) ratio on the initial porosity of the ITZ and bulk cement pastes [12,13]. The cement particles are represented as solid spheres, with a center and a radius, as described above. For simulations without hydration taking place, this is actually a more accurate way to place the particles around the aggregate surface. When hydration takes place, then the system must be sub-divided into pixels in order to allow the digital-image-based hydration code to work [8].

Figure 1 shows graphs of initial porosity vs. distance from an aggregate surface for a random particle packing of two different cements and three different w/c ratios. The computational volume consisted of a three-dimensional box 200 μm on a side. Because of the inefficient packing of the cement particles near the aggregate surface, the ITZ cement paste is observed to contain much less cement and much more water-filled capillary porosity than the cement paste far away from the aggregate surface. This inefficient packing of cement particles, the so-called "wall effect," is one of the major reasons for the formation of the ITZ in cement-based composites [1].

The results of this modelling indicate that the extent of the ITZ corresponds closely to the median cement particle diameter on a mass basis (28 μm for Cement A1 and 11 μm for Cement A7, respectively). What is meant by the "extent" or "thickness" of the ITZ is that distance over which the porosity is significantly greater, by a factor of 10% or more, than the bulk porosity. The w/c ratio does not appear to affect the thickness of the ITZ region (as we are ignoring any effects of bleeding). The w/c ratio does however appear to affect the porosity gradient, which will alter both the ITZ and bulk cement paste w/c ratios, in the following manner.

The competition between ITZ and bulk cement paste plays a major role in determining the properties of a concrete, as will be shown later in this chapter. There is clearly less cement in the ITZ regions. The w/c ratio in the ITZ cement paste must then be higher than the overall w/c ratio. The w/c ratio in the bulk (non-ITZ) cement paste must then be lower than this overall value, because the average or overall w/c of the concrete has been fixed by choosing the initial masses of water and cement to be mixed with the aggregates. If these masses are conserved during the mixing and curing process, then the average w/c must be fixed. Therefore, a region of higher than average w/c ratio implies that there must exist a region of lower than average w/c ratio. This realization is

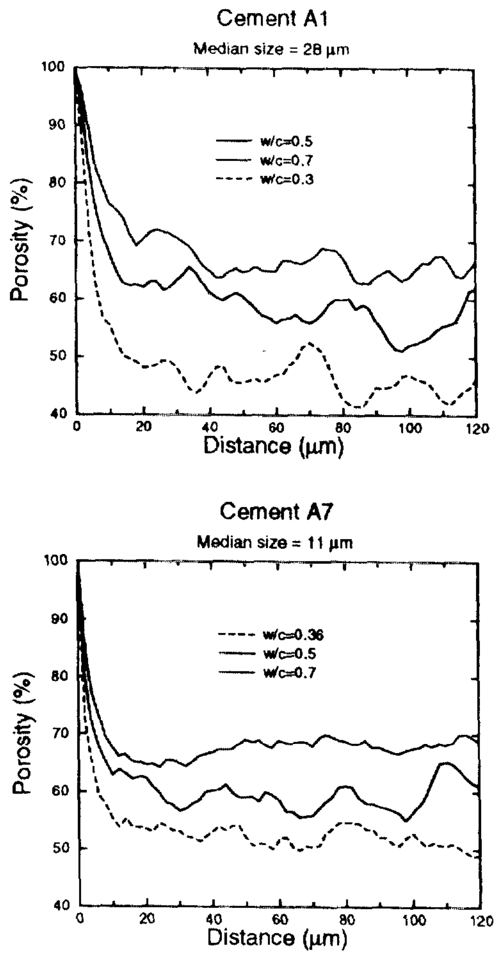

Figure 1: Porosity fraction near aggregate surface prior to hydration for two different cements (reprinted from Ref. 13). The median cement particle diameters of the two cements are: A1 - 28μm, A7 - 11 μm.

critical in the interpretation of experimental measurements of transport properties of mortars and concretes, as will be discussed further below (see Section 4).

For digital-image-based simulations of single ITZ microstructure, a simple geometry, such as a square or flat plate in 2-D or a cube or thin plate in 3-D, is generally used to represent the aggregate. The essential point is that the radius of curvature of the aggregate surface be much larger than the typical cement particle radius of curvature. This is because the typical aggregate diameter is much larger than the typical cement particle diameter (300-500 µm vs. 10-20 µm). Figure 2 illustrates a two-dimensional microstructure before and after hydration, using a flat plate aggregate (radius of curvature is infinite). Once an aggregate is placed in the microstructure, the cement particles are placed at random locations, such that they do not overlap any portion of the aggregate. The simple geometries used for the aggregates facilitate the subsequent quantification of ITZ microstructure, specifically the determination of the phase fractions present as a function of distance from the aggregate surface.

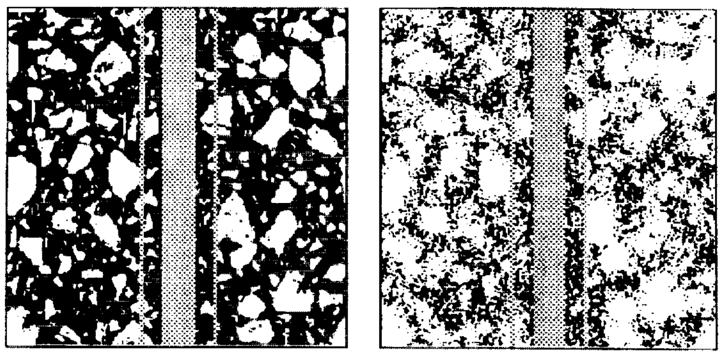

Figure 2: Original (left) and 65% hydrated (right) ITZ microstructures. The aggregate is gray, and all cementitious materials, hydrated and unhydrated, are white, with black representing water-filled porosity. The space between the thin gray vertical bars and the aggregate is the approximate extent of the ITZ region.

In addition to the wall effect contributing to the microstructure of the ITZ, digital-image-based simulations have identified a secondary mechanism active in ITZ formation, the so-called "one-sided growth" effect [14]. As hydration occurs in regions far away from an aggregate surface, the porosity is filled in with hydration products coming from all directions. However, near an aggregate surface, reactive growth occurs only from the cement paste side. Using computer simulations, this effect was isolated and quantified by allowing the initial cement particles to freely overlap the aggregate surface, thus eliminating the wall effect. While the wall effect typically scales with the median diameter of the cement particles, the one-sided growth effect appears to be active only over a distance of a few micrometers, at most. In addition to studying formation mechanisms, digital-image-based simulations have also been employed to study the effects of mixing and flocculation on the initial distribution of cement particles near an aggregate surface [15].

3.1.2 ITZ Microstructure During Hydration

Operating on an initial cement distribution (as described above), using the full portland cement chemistry [8] in a digital-image-based hydration model, the volume fraction of the hydrated phases can be studied in the ITZ region.

Figure 3 shows a plot of the phase distributions as a function of distance from the aggregate surface for a w/c=0.45 cement paste with a degree of hydration of 70%. The degree of hydration is defined as the total mass of cementitious material reacted divided by the initial value of this quantity [8]. These phase distributions are in good qualitative agreement with numerous experimental measurements of these phase gradients, such as those presented by Scrivener and Pratt [16]. In general, the model results strongly support the experimental results and interpretations of Breton et al. [17], which are largely based on the earlier work of Maso [1]. Ions with a relatively high mobility in cement paste pore solution, such as Ca^{++}, Al^{3+}, and SO_4^{2-}, tend to diffuse into the more porous ITZ (due to concentration gradients arising from the initial higher w/c ratio in the ITZ), resulting in the precipitation of calcium hydroxide (CH) and aluminate hydration products such as ettringite. Because silicate and ferrite ions have lower mobilities, they tend to form hydration products near their dissolution source. Thus, since the ITZ is generally deficient in anhydrous cement, it will also exhibit lower phase volume fractions of calcium silicate hydrate (C-S-H) gel and iron hydroxide. While hydration does tend to reduce the porosity gradient near the aggregate surface, it still exists as a prominent microstructural feature which will influence both strength and durability. Many of these microstructural features observed in ITZ regions between the aggregates and the cement paste matrix have also been found to exist in steel reinforcing bar-cement paste interfaces [18,19].

Because a complete representation of the microstructure is available as an output from the hydration model, one can also calculate other experimentally measurable quantities such as the Ca/Si molar ratio. Several researchers have used electron probe microanalysis to study this ratio within the ITZ and bulk cement pastes [20-22]. Figure 4 shows a plot of Ca/Si for a 0.45 w/c ratio computer model tricalcium silicate (C_3S) paste after 77% hydration. The Ca/Si ratio is seen to settle down to its expected bulk value of 3 (for pure C_3S) at a distance roughly corresponding to the average cement particle diameter used in the initial microstructure (16 pixels or µm). Approaching the aggregate surface, this ratio increases monotonically to a maximum value slightly larger than 5. This result is in excellent agreement with the experimental observations of Larbi and Bijen [21], who observed a maximum value of about 5 for a 28-day old ASTM Type I portland cement paste with w/c=0.40, and Yuan and Odler [20], who measured a maximum value of just over 6 for a hydrated pure C_3S paste with w/c=0.38. Since this value would initially be constant everywhere, on average, these model and experimental results support the hypothesis that calcium ions are diffusing into ITZ regions at a much faster rate than the silicate ions [1,17].

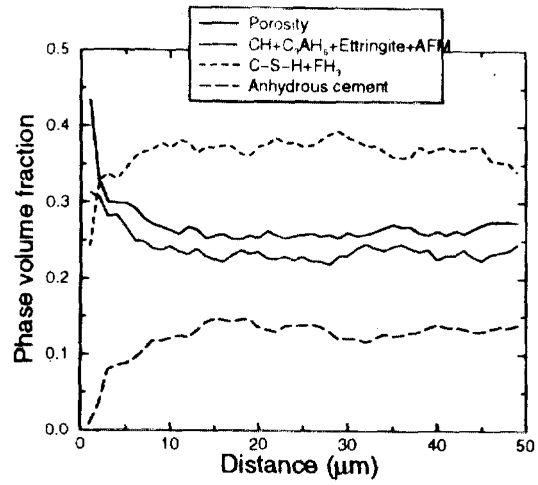

Figure 3: Phase fractions vs. distance from aggregate surface, w/c=0.45, 70% hydration.

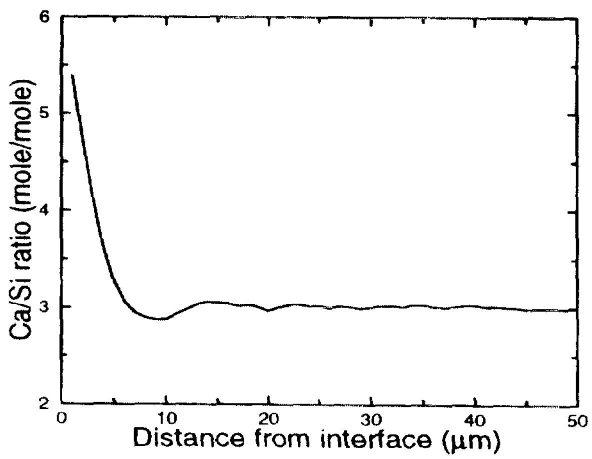

Figure 4: Ca/Si ratio vs. distance from aggregate surface for C_3S paste, w/c=0.45, 77% hydration. (Adapted from Ref. 23).

3.1.3 Effects of Mineral Admixtures

From the above results, one way of improving the microstructure of the ITZ might be to increase the concentration of silicate ions in this region. Here, "improvement" means reducing the width of the ITZ or reducing the porosity gradient in the ITZ or both. The addition of mineral admixtures is one approach that has been successful in improving the microstructure of the ITZ. Computer simulations have been performed to study the effects of various mineral admixture characteristics on the ITZ microstructure. This has been done approximately, for C_3S only pastes [24]. To do this, a portion of the cement is replaced with a mineral admixture (e.g., silica fume or fly ash) that is allowed in the hydration model to consume a portion of the CH, resulting in the formation of additional (pozzolanic) C-S-H. A pozzolanic reactivity specifies how much CH can be consumed per unit volume of mineral admixture. This value would typically be larger for silica fume than for fly ash, due to the higher silica content of silica fume. Silica fume is modelled as one-pixel particles, the smallest size available in the digital-image-based model, even though silica fume particles are typically somewhat smaller in diameter than the 1 μm represented by a single pixel. Fly ash is usually similar in size to the cement particles, although beneficiation can be utilized to separate out the finest portion of a fly ash, to increase its effects on properties like strength development [25-28].

Several mineral admixtures used in concrete, such as silica fume, fly ash, and more recently rice husk ash [29], influence the ITZ microstructure both through their size and through their pozzolanic reactivity [24,30] (blast furnace slag has not yet been modelled using this approach). When the mineral admixture particles are much smaller than the cement particles, such as is the case for a well dispersed silica fume, they help significantly in offsetting the "wall" effect, thus reducing the width of the ITZ. Recall that it was previously shown that the ITZ width scaled as the median particle diameter, so that using smaller particles in place of some of the cement particles will reduce the width of the ITZ. In addition, due to their silica content, the mineral admixture particles often react with the calcium ions diffusing into the ITZ to produce pozzolanic C-S-H, as opposed to the conventional precipitation of large CH crystals in the ITZ.

To study the interaction between mineral admixture size and pozzolanic reactivity, the microstructural development for model 3-D C_3S systems containing mineral admixtures with various size and reactivity combinations was studied [23]. The aggregate was a 100^3 cubic pixel particle, and was embedded in a 200^3 cubic pixel computational cell. The ITZ, with no mineral admixtures, was clearly seen to be a region deficient in cement and C-S-H while containing a relative abundance of porosity and CH. The addition of the mineral admixtures was seen to significantly alter this "base" microstructure. For example, the addition of 20% silica fume resulted in a much denser and more homogenous microstructure, in agreement with a number of experimental observations on the effects of silica fume on ITZ microstructure [23,31-33]. However, when the silica fume particles were agglomerated, they were much less effective in improving ITZ microstructure. Thus, proper dispersion of silica fume is needed to assure optimum performance [34].

A quantitative analysis of six microstructures is presented in Fig. 5, which provides a graph of the cement + C-S-H phase fractions vs. distance from the aggregate surface for each of the systems studied in Ref. [23]. These two phases have been combined based on the hypothesis that they are most important in strength development. In Fig. 5, for the system with 20% replacement with small silica fume particles, this composite phase fraction increases in the bulk paste. The ITZ porosity gradient is also greatly reduced. The system with large silica fume particles corresponds to the agglomerated silica fume discussed above. Fly ash is less beneficial than silica fume in this respect, due to both its larger size and its lower pozzolanic reactivity. However, the system utilizing small reactive fly ash particles offers a performance comparable to the large (agglomerated) silica fume system, emphasizing both the importance of proper dispersion and the advantages of beneficiation. Color cross-sections of all these systems can be found at http://ciks.cbt.nist.gov/garbocczi/, Chapter 6, Section 2.

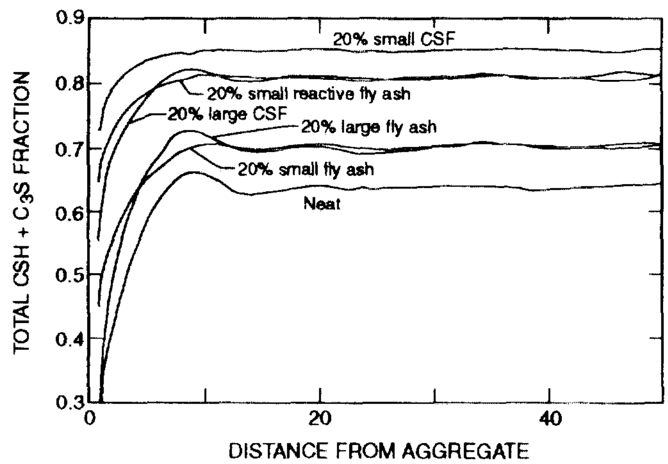

Figure 5: Total C-S-H + C_3S + mineral admixture fraction, as a function of distance from aggregate surface for plain and admixture-modified C_3S pastes with water/solid ratio = 0.45 at 77% hydration. (Reprinted from Ref. 24).

3.1.4 Effects of Aggregate Characteristics

Digital-image-based computer models can also be used to study the effects of aggregate characteristics, such as sorptivity and reactivity, on ITZ microstructure. For sorptivity, the major practical example would be the use of absorptive lightweight aggregates in concrete. Several researchers have observed that the ITZ in lightweight aggregate concrete is denser than that in ordinary concrete and may be even denser than the bulk paste microstructure [35,36]. Fagerlund has suggested that this phenomenon is caused by the lightweight aggregates acting as filters or sponges, drawing in water and pulling cement particles towards their surfaces [37]. This effect can be easily simulated by moving all cement particles a prescribed distance towards the aggregate surface, as shown in Fig. 6, to simulate water absorption by the unsaturated aggregate. This results in an increase in cement volume fraction near the aggregate surface, partially offsetting the wall effect.

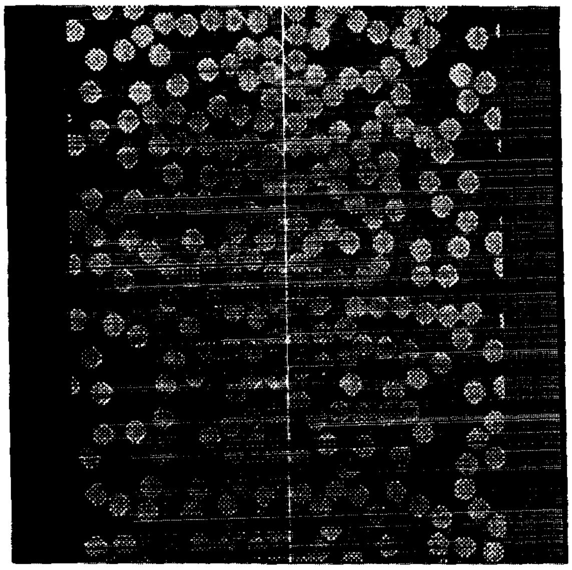

Figure 6: Initial microstructure of gray C_3S grains (after absorption) for an absorptive aggregate (thin middle white line). The cement particles have been drawn in towards the absorptive aggregate in the middle of the picture. (Adapted from Ref. 13).

Figure 7 provides a plot of the hydrated cement paste phase fractions averaged over five 2-D C_3S systems for the cases of normal and absorptive aggregates [13]. Both the C_3S + C-S-H volume fraction and the porosity exhibit improvements in the case of the absorptive aggregate, implying a denser and more homogeneous ITZ. Due to the one-sided growth effect and the finite size of the cement particles, there is still an ITZ in the case of the absorptive aggregate, but its size is definitely reduced relative to that of the normal aggregate concrete. In a real concrete, the roughness of the lightweight aggregate might also play a role, as the irregularly shaped cement particles may be drawn tightly against the aggregate surface in a "lock-and-key" fashion, improving the microstructure as well as providing a larger degree of mechanical interlock than when using normal density aggregates.

Absorptive aggregate

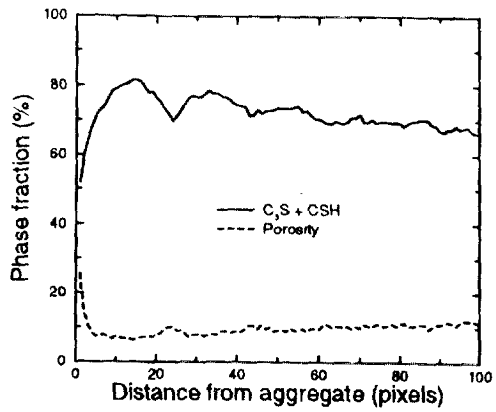

Normal aggregate

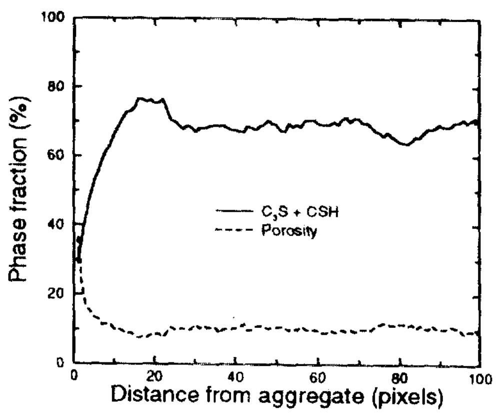

Figure 7: Quantitative phase analysis for absorptive aggregate microstructure, w/c=0.39, 77% hydration. The normal aggregate data is included for comparison. (Adapted from Ref. 13).

In addition to sorptivity, another aggregate characteristic that may be studied using the model is reactivity. Experimentally, Berger [38] has prepared concrete using cement clinker as aggregate and attributed the observed increase in compressive strength to an improved paste-aggregate bond. In addition to absorbing some water due to its inherent porosity, the clinker aggregate will also hydrate at its surface, eliminating the one-sided growth effect. Figure 8 shows a hydrated microstructure for a 2-D C_3S system containing a model clinker aggregate. The quantitative analysis provided in Fig. 9 indicates a marked improvement in ITZ microstructure, as there is no evidence of a porosity gradient, and the C_3S + C-S-H phase fraction actually increases slightly as the interface is approached. The simulation studies also suggest that a thin reactive surface layer should be sufficient to achieve this microstructure improvement, as supported by a number of recent experimental studies [39-42]. This concept of a surface reactive layer has also recently been extended to MDF cement systems, in an attempt to improve the moisture resistance of this class of cementitious materials [43].

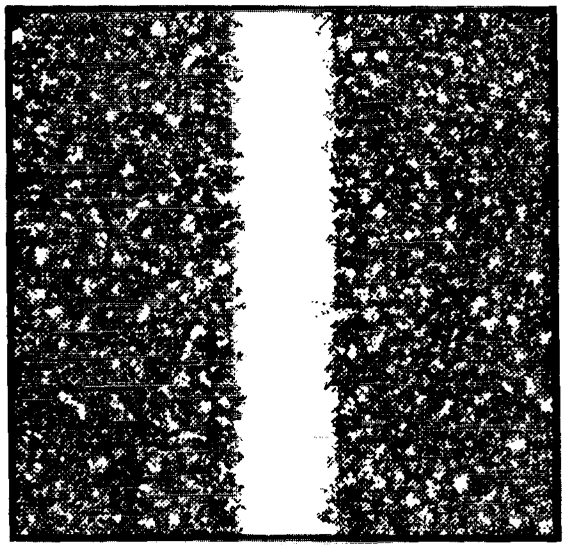

Figure 8: Hydrated microstructure for an absorptive clinker aggregate, w/c=0.39, 75% hydration. Color scheme is: white-C_3S, light gray-CH, dark gray-C-S-H, and black-porosity (adapted from Ref. 13).

The model has also been applied to the case of a non-reactive aggregate that serves as a precipitation surface for the formation of C-S-H. The results provided in Fig. 10 indicate that in this case, the porosity gradient will be reduced in the immediate vicinity of the aggregate surface, but the overall width of the ITZ will remain relatively constant. These examples illustrate the power of using computer modelling to study a wide variety of scenarios and their influence on ITZ microstructure.

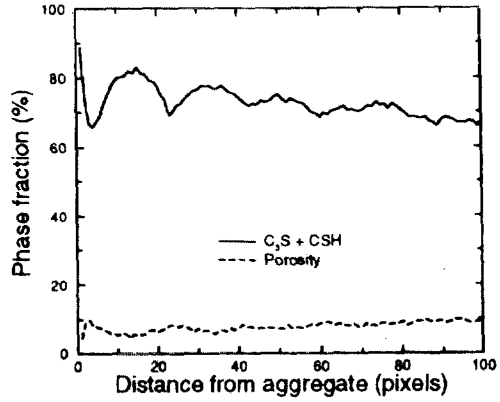

Figure 9: Quantitative phase analysis for absorptive clinker aggregate microstructure, w/c=0.39, 75% hydration. (Adapted from Ref. 13).

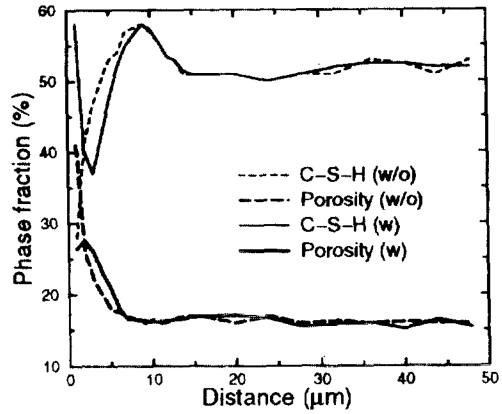

Figure 10: Quantitative phase analysis for non-reactive aggregate systems without (w/o) and with (w) precipitation of C-S-H on aggregate surface, w/c=0.41, 70% hydration.

3.2 Many Aggregate Models

A real concrete is composed of more than 50% by volume of aggregates, and thousands of aggregates per cubic centimeter, implying the existence of many local ITZ regions, which comprise a material phase *different* from the bulk cement paste. The first aspect of this new complicated material phase to be studied is the connectivity or percolation of these ITZs in a mortar or concrete. The percolation of these ITZ regions, or specifically the capillary porosity contained in the ITZs, through a concrete was first indicated by mercury intrusion porosimetry data [44,45] and has more recently been inferred from SEM observations of specimens intruded with Woods' metal [46]. This percolation of the individual ITZs would be expected to influence transport properties, as the large pores present in the ITZs offer much less resistance to the diffusive and convective transport of aggressive species into the concrete. Any such effect of the ITZ regions is of course in competition with the presence of aggregates, which tend to reduce the volume of pathways and increase the path lengths for transport. This competition will be explored more fully in the transport section below (Section 4).

The percolation of ITZs can be examined using a hard core/soft shell (HCSS) model [47], first adapted to concrete by Winslow et al. [48], and later duplicated by Bourdette et al. [49]. This is a continuum model. The model has also been employed by Johansen and Thaulow [50] to estimate the volume of reactive aggregate (sand) which can be present in concrete without causing deleterious expansion. In the HCSS model, the aggregates are represented by a collection of impenetrable spheres that follow a measured particle size distribution. Each aggregate is surrounded by a concentric spherical shell that represents the ITZ. In general, the thickness of the ITZ is not a function of aggregate particle size, as was discussed above, but is instead controlled by the median size of the cement particles (see Ref. [51] for further discussion of this question). Typical computational volumes are 1000 mm^3 for mortar and 27,000 mm^3 for a concrete, which requires on the order of 1,000,000 individual aggregate particles for the concrete systems.

For mortars, the model has been calibrated against experimental mercury intrusion porosimetry data [48] that indicated a large increase in the volume fraction of porosity intruded by mercury at low pressures when the sand content of the mortar was increased from 44.8% to 48.6%. This increase in "coarse" porosity could be indicative of a percolation transition for ITZ connectivity. Using the same sand particle size distribution as that employed experimentally, simulations were conducted for different sand contents and values of ITZ thicknesses ranging from 10 to 40 μm. Figure 11 provides a plot of the results, showing the fraction of the ITZ volume that is part of a percolated pathway through the 3-D microstructure as a function of sand content and ITZ thickness. From this plot, one can observe that an ITZ thickness of 15-20 μm best agrees with the experimental observations of a large increase in connectivity in the range of 45-50% sand. This value is smaller than the 40-50 μm typically estimated using SEM techniques [23,31,32], but this would be expected since the largest pores in the ITZ should be those nearest to the aggregate surface, where the porosity gradient is steepest (see Fig. 3). Thus, the measured thickness of the ITZ will depend on the experimental technique being employed.

The second feature of the ITZ phase is its volume fraction. The HCSS model can be used to determine the fraction of cement paste within a given distance of an aggregate

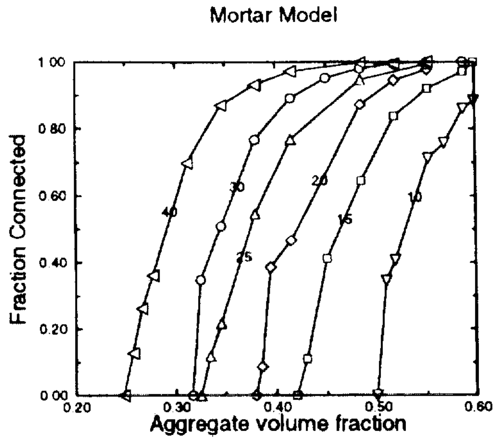

Figure 11: Percolated ITZ volume fraction vs. aggregate content for various ITZ thicknesses in μm (adapted from Ref. 48).

surface, thus giving the volume fraction of the ITZ regions as a function of their thickness. This is done using a numerical point-counting technique [48]. Using measured aggregate size distributions for mortar [48] and concrete [45], results shown in Fig. 12 indicate that nearly all of the cement paste is within 100 μm of an aggregate, consistent with the SEM-based observations of Diamond et al. [52]. Also, 20-40% of the total cement paste is within the typical ITZ thickness of 20-30 μm. This volume fraction of ITZ paste is more than sufficient to create a percolated pathway through a

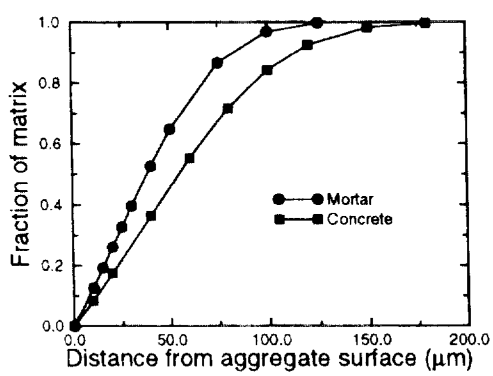

Figure 12: Fraction of total cement paste volume that lies within a given distance of an aggregate surface for a mortar with a sand volume fraction of 0.552, and a concrete with an aggregate volume fraction of 0.646.

microstructure, suggesting that most real concretes will contain percolated ITZ regions. It has been found recently that this prediction of the HCSS model can also be carried out analytically, with great accuracy, using a result of Lu and Torquato [51,53,54] (see section 4.2.1), when the aggregates are spherical.

The HCSS model has been extended to the case of elliptical particles of various aspect ratios [4]. Figure 13 provides a plot of ITZ connected fraction vs. sand volume fraction for systems with five different choices of semiaxis length combinations a:b:c. One can clearly observe that smaller volume fractions of the elliptical particles are needed to achieve percolation of the ITZ regions. This is mainly due to the increased surface area per volume ratio of an ellipsoid relative to a sphere [55]. Figure 14 shows how these connectivity values for different aspect ratios collapse onto a single curve (for a fixed ITZ thickness) when plotted against the surface area of the aggregate, corrected slightly for the non-uniform thickness of the ITZ layer when ellipsoidal particles are employed [4]. ITZ thicknesses of 50, 22.5, and 10 μm were used in Fig. 14.

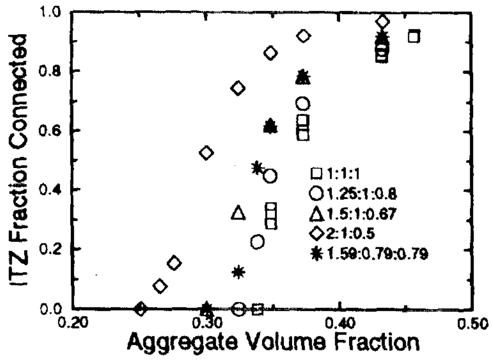

Figure 13: Percolated ITZ volume fraction vs. aggregate content. Three data sets are shown for the 1:1:1 aspect ratio to provide some indication of variability. The ITZ thickness is 22.5 μm.

Figure 15 compares the spherical and ellipsoidal particle modes by showing cross-sections from two 3-D mortar models of these types. This figure also serves to illustrate an important difference in percolation characteristics between 2-D and 3-D. In a 2-D slice, the ITZ regions do not appear to be percolated, while in fact they are percolated in 3-D. One cannot determine 3-D percolation quantities by looking at 2-D models or 2-D slices of 3-D materials.

Scaled surface areas

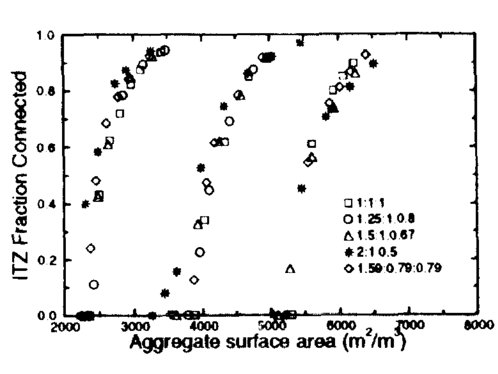

Figure 14: Percolated ITZ volume fraction vs. aggregate surface area for ITZ thicknesses of 50, 22.5, and 10 μm (from left to right).

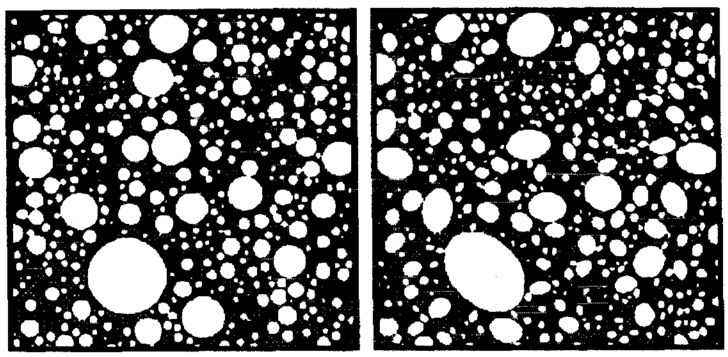

Figure 15: Two cross sections from 3-D mortar models, using spherical agregates-left, and ellipsoidal aggregates-right. Gray is bulk cement paste, white is aggregates, and black is ITZ regions.

Having used percolation ideas applied to the HCSS model, coupled with various numerical techniques, to establish some idea of the geometry and topology of the ITZ phase in a concrete, the focus now turns to quantifying the effect of the ITZ phase on concrete transport properties.

4. Transport Properties

Because of the wide range of feature sizes in concrete, from nanometer-sized pores to millimeter-sized aggregates, memory limitations on current computers make it impossible to simultaneously represent all of these structural features in a single microstructure model. For example, suppose one wanted to represent all phases, from C-S-H to aggregate, in a 3-D digital image model of concrete. The pixel size in this case should be one nanometer, which would be barely adequate for the resolution of the C-S-H phase. The minimum size model that would incorporate enough aggregates to be statistically valid would be at least 30 mm on a side, assuming a maximum aggregate size of about 10 mm. Such a model would contain $(30 \times 10^6)^3 = 2.7 \times 10^{22}$ pixels! Considering the limits of even modern-day computers, uniting multiple length scales in a single model in a more sophisticated (and less computer-memory intensive!) way is obviously necessary.

Multi-scale modelling techniques offer a promising solution to this restriction [56,57]. In this approach, properties computed at one scale, say micrometers, are fed into a model which is constructed at a higher scale, such as millimeters. The present multi-scale model combines microstructure models for the cement paste surrounding a single aggregate (micrometers), and for a representative volume of concrete (millimeters). These two microstructure models are used, in association with computational techniques for computing the diffusivity of a three-dimensional microstructure, to compute the diffusivity of a representative volume of concrete. This procedure was first demonstrated for mortars [57], and has since been extended to normal concretes [6,51]. The equation used for diffusivity at the micrometer scale also indirectly incorporates information from the nanometer scale, so that 6-7 orders of magnitude of length scale are actually contained in the model.

Computation of the transport properties of a concrete is made difficult by the fact that two length scales must be treated directly: the micrometer scale ITZ regions, and the millimeter scale aggregates. In Refs. [58] and [59], it was shown how to compute the overall diffusivity of a concrete model, where the difference between bulk and ITZ cement paste could be quantitatively taken into account. In that paper, it was mentioned that the redistribution of cement between bulk and ITZ regions, because of the different w/c ratios in these regions, could very well be important, and would have to be considered in future models. The main reason for this particular multi-scale approach being developed [6] was to approximately handle this redistribution of cement between ITZ and bulk cement paste. This effect does indeed turn out to play an important role in predicting concrete diffusivities, because it affects what diffusivity values need to be assigned to the bulk and ITZ phases in a composite analysis of concrete properties. Therefore, the results of Refs. [58] and [59] are incomplete, and need a multi-scale analysis in order to properly assign values to the diffusivity of various phases.

In Ref. [6], this multi-scale modelling approach was extensively discussed, showing how different length scales could be quantitatively linked to predict the diffusivity of a concrete material. Because of the complexity of the problem, several key steps used in generating the model results had to originally be based on large-scale computer simulations, using supercomputing-type computing power. It was hard to change parameters, because of the long run times involved. Also, the computing power necessary to solve the model would be unavailable for most concrete technologists. In Ref. [51], it was shown how two out of the three key steps in the multi-scale model could be accurately replaced with analytical expressions. This section will briefly present the fundamental aspects of the multi-scale diffusivity model, leaving details to the references.

The multi-scale model, as developed, has some limitations. The model applies to conventional ($0.25 < w/c < 0.75$), fully-saturated concretes. Diffusion/sorption in partially saturated concrete is important in many field exposures but is not addressed in this study. In addition, only ionic diffusion under steady-state conditions is considered, with the short time effect of chloride binding ignored. Mathematically, this is equivalent to electrical and thermal conductivity, so this analysis applies to these areas as well [60]. Also, only concrete without mineral admixtures can be presently handled.

However, the presence of entrained air bubbles is allowed. Air voids are considered to be equivalent to aggregate particles in terms of their effects on ionic diffusivity. They are assigned a diffusivity of 0 and an associated ITZ region like the aggregates [61]. It is assumed that the air voids are not filled with water. Concrete exposed to water for a long period of time may actually have the air voids filled with water. A fixed air void size distribution is used for all of the simulations based on a logarithmic probability density function [62]. Air voids smaller than 100 micrometers in diameter are not included in the model, however, as they are similar in size to the cement particles. The whole concept of the ITZ breaks down when the cement grains are similar in size to the aggregates, so that this small size air bubble cannot be handled with this methodolgy. Avoiding this size range air bubble should not significantly affect results, however.

4.1 Multi-scale model

In the approach to computing the diffusivity of concrete that has been previously discussed [58,59], the ratio of the concrete diffusivity to the bulk cement paste diffusivity as a function of the ITZ diffusivity and the aggregate volume fraction was computed. The value of diffusivity produced was relative to the value assigned to the bulk paste phase.

One might then naively think that an analogous experimental measurement would be to measure the concrete diffusivity as a function of the degree of hydration, and also measure the diffusivity of the cement paste from which the concrete was made (same w/c ratio). Normalizing the concrete diffusivity by the cement paste diffusivity at the same degree of hydration would presumably then give a number that could be compared to the model number [58,59]. As was pointed out in Ref. [58], this approach is not entirely correct. The main reasons are the way concrete is made, and the way in which the interfacial transition zone, as mentioned earlier, serves to redistribute the cement. There is, therefore, a higher than average w/c ratio in the ITZ regions and a lower than average w/c ratio in the bulk regions. The following example will serve to illustrate this point more precisely.

Suppose a concrete was made by mixing a 0.5 w/c cement paste with enough aggregates so that the final volume fraction of aggregates is 60%. We assume here that the aggregates neither absorb nor give off water. If the ITZ is 20 μm thick, all cement paste within this distance from an aggregate will, on average, have a higher porosity and therefore a w/c ratio higher than 0.5. This is because there is known to be less cement in the ITZ than in the bulk paste [48,63]. But the only way this can happen is for the cement paste outside the ITZ region to have a w/c ratio that is less than 0.5 and, therefore, a lower porosity, since the average w/c ratio has been specified to be 0.5 by the initial mixing conditions. If the ITZ volume fraction is small, this effect is also small, which would be the case for a small aggregate volume fraction. However, as the volume fraction of aggregate increases, the ITZ volume fraction also increases, and this effect can become quite appreciable. So for this hypothetical concrete, it would be incorrect to consider an 0.5 w/c ratio cement paste to be the matrix or bulk phase for the concrete. The actual bulk paste, where "bulk" means outside the ITZ region, would have a lower w/c ratio, possibly as low as 0.4. Therefore, concrete is *not* a simple two-phase composite, of cement paste plus aggregates, and not even a simple three-phase composite, of aggregates plus interfacial transition zone and bulk cement paste. Concrete is rather an *interactive composite*, where the amount of the aggregates influence the properties and amounts of the cement paste phases. The multiscale model approach described in this paper is designed to approximately take this effect into account, by combining models to actually compute this redistribution of cement and w/c ratio.

The multi-scale model works in three steps. It is not a particularly simple model, as it is addressing the transport properties of a complex interactive composite material.

(1) The cement particle size distribution (PSD) is used to establish the interfacial zone thickness, t_{ITZ}. The value of t_{ITZ} is taken to be equivalent to the median cement particle diameter, ignoring any effects of bleeding [13]. The first key step is then, using the millimeter-scale concrete microstructure model, to place aggregate particles, following the aggregate PSD of interest, into the concrete volume. Systematic point sampling is then used to determine the volume fractions of interfacial transition zone (V_{ITZ}) and bulk (V_{bulk}) paste for this particular choice of aggregate PSD and value of t_{ITZ} [48].

(2) The second key step uses the micrometer-scale cement hydration model. The shape of the model volume is shown in Fig. 16, with aggregate, ITZ, and bulk paste regions defined. We want to determine the local microstructure near a single aggregate surface, in order to be able to compute the contrast between ITZ and bulk paste diffusivities. The dimensions of the model box are chosen to match the ratio of V_{ITZ}/V_{bulk} (determined in step 1). By matching the ratio V_{ITZ}/V_{bulk} as determined in the concrete volume, we approximate the microstructure that exists near a typical aggregate surface.

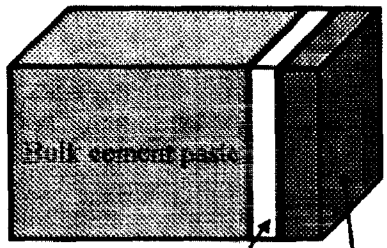

Figure 16: Showing the breakdown, in the cement hydration computational volume, of aggregate (black), interfacial zone cement paste (white), and bulk cement paste (gray). The ratio V_{ITZ}/V_{bulk} is about 0.16 in this figure.

Cement particles are placed into this computational volume, following the cement PSD, to achieve the specified total w/c ratio. Of course, the w/c ratios in the two regions will be different because of the wall effect of the aggregate surface. The actual numerical difference is a prediction of the micrometer-scale microstructure model, and is not specified by the user. The cement particles are then hydrated, using the model, up to a desired degree of hydration. After hydration, the porosity ϕ is measured as a function of distance from the aggregate surface. The relative diffusivity, D/D_o, of cement paste as a function of distance from the aggregate surface, x, can be estimated using a previously established relationship [64]:

$$\frac{D}{D_o}(x) = 0.001 + 0.07\phi(x)^2 + 1.8H(\phi(x) - 0.18)\,(\phi(x) - 0.18)^2 \qquad (1)$$

where relative diffusivity is defined as the ratio of the diffusivity D of ions in the material of interest relative to their value in bulk water, D_o, $\phi(x)$ is the capillary porosity volume fraction at a distance x from an aggregate surface, and H is the Heaviside function having a value of 1 when $\phi > 0.18$ and a value of 0 otherwise. This equation comes from fitting the results of several different w/c cement pastes at many different degrees of hydration, where a value of diffusivity for the C-S-H phase was used which roughly agrees with nanometer scale simulations of C-S-H nanostructure and properties

[56]. The constant term in eq. (1) comes from the limiting value of diffusion through C-S-H gel pores when the capillary porosity is zero. The H term represents diffusion through percolated capillary porosity, and turns off this transport mechanism when the capillary porosity percolation threshold is reached. The second term in eq. (1) is a fitting term that connects the two limiting behaviors [64]. Equation (1) is not exact, of course, but should give results accurate to at least a factor of two for the absolute diffusivity, and better than that for ratios of ITZ to bulk diffusivity, for the usual range of capillary porosity encountered (10-40%). Refs. [64,65] give experimental validation of this model and the associated eq. (1).

Using eq. (1), the diffusivity as a function of distance from the aggregate surface is computed. These diffusivity values are averaged in two subsets, those lying within a distance t_{ITZ} of the aggregate and those in the "bulk" paste, to give two values, D_{ITZ} and D_{bulk}. Averaging in this way assumes that the diffusive flux in the two phases is locally parallel to the aggregate surface, and so each layer can be simply summed up. By averaging over t_{ITZ}, the simplifying approximation is made that the interfacial transition zone has a fixed width with fixed properties. The average over the simulated local microstructure of the interfacial transition region is done to help make this approximation more accurate. Choosing a different value of t_{ITZ} would of course give a different value of ITZ diffusivity. Other ways of averaging over the local microstructure are possible, such as matching to an exact solution of a single specific size aggregate with a gradient of properties around it [66]. These methods do not, however, seem to make a significant difference in the final results [66].

After the first two steps, we now have a microstructure model of the concrete, using spherical aggregates that follow the correct PSD, and we have values of diffusivity for each of the three phases in the concrete: aggregate ($D_{agg} = 0$), bulk cement paste (D_{bulk}), and ITZ cement paste (D_{ITZ}). It is crucial to remember that the values of D_{bulk} and D_{ITZ} were determined interactively, since the amount and size of the aggregates was used to determine the value of V_{ITZ}/V_{bulk} that was used in the cement paste model, which in turn helped determine the value of D_{ITZ}/D_{bulk}. The ratio of D_{ITZ}/D_{bulk} is a function of the aggregate PSD and volume fraction and the degree of hydration of the cement.

(3) The third key step is to finally use the ratio of the bulk and ITZ cement paste diffusivities, D_{ITZ}/D_{bulk}, as an input back into the original diffusivity concrete model [58,59]. Random walk numerical techniques are then employed to compute the diffusivity of the overall concrete system. The random walker techniques employed for this calculation have been previously described [58,59]. These techniques are quite computer-time intensive, but do not use huge amounts of memory. The relative diffusivity of the concrete, D_{conc}/D_{bulk}, is calculated by this algorithm [57-59]. This value can then be converted into an absolute chloride ion diffusivity for the concrete, D_{conc}, by multiplying it by D_{bulk}/D_o determined from the cement-level microstructural model [eq. (1)] and by D_o, the diffusion coefficient of chloride ions in bulk water at room temperature (25°C), given as 2.0×10^{-9} m^2/s [67]. By changing the value of D_o to

correspond to that measured for the specific ion of interest, the above techniques can be generalized to other ionic species of relevance in cement-based materials. This model does not address effects such as chemical binding and chemical reactions of the diffusant.

4.2 Analytical methods

The first and third key steps of the multi-scale model, as described above, can be accurately replaced by analytical equations. This allows computer power and runtimes needed to compute the model to be greatly reduced, and brings the whole model within range of a high-end PC or a low-end workstation.

4.2.1 Interfacial zone volume: Step (1)

An analytical estimate for the total interfacial zone volume around a collection of spheres of various sizes can be obtained from the literature on the statistical geometry of composites [53]. In this work, a collection of spheres of various sizes are randomly placed in a volume according to ***equilibrium*** statistics. These involve treating the spheres as being dispersed in a liquid, where the effect of gravity is neglected, and allowing them to be "shaken" sufficiently to achieve their desired positions. This process is actually similar to how a real concrete is mixed. In the case of the concrete model, however, the particles are placed according to non-equilibrium random parking statistics [68], as described above. However, this analytical formalism works quite well for the concrete model [51,54].

There are many analytical results contained in the paper by Lu and Torquato [53] that are relevant to the concrete problem. In this paper we focus on the quantity $e_V(r)$, the "void exclusion probability" as denoted in Ref. [53] (note: in our case, "void" means outside the aggregates). As formulated by Lu and Torquato, if one adds a spherical shell of thickness r around each one of the spherical particles, the volume fraction of material outside of both the particles and the shells is just $e_V(r)$. The ITZ volume fraction, V_{ITZ}, is then just

$$V_{ITZ} = 1 - e_V(t_{ITZ}) - \eta \tag{2}$$

where η is the volume fraction of aggregates [53]. The functional form of $e_V(r)$ is

$$e_V(r) = (1-\eta)\exp[-\pi\,\rho\,(cr + dr^2 + gr^3)] \tag{3}$$

where ρ is the total *number* of aggregates per unit volume, and the coefficients c, d, and g are given in terms of averages (<...>) over the particle size distribution of the aggregates in terms of *number*, not volume. These averages can be determined from an aggregate sieve analysis, using certain reasonable assumptions, as is shown in Section 4.4. The coefficients c, d, and g are:

$$c = \frac{4 < R^2 >}{(1-\eta)} \quad (4)$$

$$d = \frac{4 < R >}{(1-\eta)} + \frac{12\varepsilon_2 < R^2 >}{(1-\eta)^2} \quad (5)$$

$$g = \frac{4}{3(1-\eta)} + \frac{8\varepsilon_2 < R >}{(1-\eta)^2} + \frac{16A\varepsilon_2^2 < R^2 >}{3(1-\eta)^3} \quad (6)$$

where $\varepsilon_2 = 2\pi\rho <R^2> / 3$, and A is a parameter that can have different values (0, 2, or 3) depending on the analytical approximation chosen in the theory [53]. The actual choice used may be fixed by experiment. In previous work on concrete models [51], the actual value of A used did not make much difference, but A=0 was always slightly better than A=2 or 3.

4.2.2 Differential effective medium theory (Step 3)

Most "effective medium theories" for two or more phase composites are derived in two steps. In the first step, the dilute limit of the composite, where the inclusion phases are present in small amounts in the matrix material, is solved exactly. The second step takes this exact solution for the dilute limit and uses a statistical approximation of some kind to get an analytical form for the case of arbitrary amounts of the phases.

The type of effective medium theory (EMT) that has been found useful for concrete diffusivity problems uses the differential scheme to generate the EMT, and is hereafter referred to as D-EMT. The mathematical basics are found in McLaughlin [69], and have been previously discussed in the context of concrete [51,59]. The first step in generating the D-EMT equation is to solve the dilute limit properly. In this case, the dilute limit is given by a single spherical aggregate particle, with $D_{agg} = 0$, surrounded by a spherical shell of thickness t_{ITZ}, of diffusivity D_{ITZ}, embedded in a matrix with diffusivity D_{bulk}. Diffusivity or electrical conductivity can be used interchangeably for this problem, as the mathematical structure is identical. If there is a very low volume fraction of such particles, then the diffusivity of the composite is described by the expansion

$$\frac{D}{D_{bulk}} = 1 + < m >_V \; c + O(c^2) + \ldots \quad (7)$$

where $<m>_V$ means that the slope is averaged over the *volume* distribution of the aggregates, since the expansion (7) is in terms of the aggregate volume fraction, not the number fraction. The slope m for a single size particle is given in Appendix A.

To generate the D-EMT equation, the dilute result above is used in the following way. Suppose that a volume fraction c' of aggregate has been added to the cement paste matrix, so that the total diffusivity is now D'. The current cement paste matrix volume fraction is $\varphi' = 1 - c'$. The aggregates have been "smeared" out so that the concrete is a uniform material. Suppose that a differential volume element of volume fraction dV is now taken out and replaced with aggregate. The new actual volume fraction of aggregate is not just c' + dV, since some of the material that was removed was also aggregate, but is equal to c' + dV - c'dV. The change in aggregate volume fraction is then just dc' = dV(1 - c'). The dilute limit is used to get the new diffusivity, D' + dD',

$$D' + dD' = D' + D' < m > dV \tag{8}$$

or, using the relation between c' and dV,

$$\frac{dD'}{D' < m >_V} = \frac{dc'}{1 - c'} \tag{9}$$

This equation can be integrated on the left from D_{bulk} , the diffusivity when no aggregates are present, to D, the diffusivity when the aggregates have volume fraction c, and on the right from 0 to the desired aggregate volume fraction c, with the final result

$$-\int_{D_{bulk}}^{D} \frac{dD'}{D' < m >_V} = \ln(1 - c) \tag{10}$$

In eq. (10) D' replaces D_{bulk} in the expression for $<m>_V$ (see Appendix A of Ref. [51]), so that $<m>_V$ is a function of D'. To obtain the predicted value of D for any value, c, of aggregate volume fraction, one simply varies the value of D until the left hand integral equals the desired value of ln(1-c).

There is one complication of this three-phase model, compared to two-phase models [69]. In two phase models, in the D-EMT process, the diffusivity of the inclusion would remain invariant, while only the matrix diffusivity would change. In this three-phase case, there is the question of whether the ITZ diffusivity, D_{ITZ}, is also renormalized in the D-EMT process, or whether it should stay invariant. The ITZ phase is outside the aggregate volume, and so must be considered part of the matrix phase. Intuitively and physically, there are two extremes that are worth considering. One is that the actual value of D_{ITZ} remains invariant. The other is that the value of D_{ITZ}/D' remains constant at what the original value, D_{ITZ}/D_{bulk}, was chosen to be. If the concrete diffusivity is being reduced with the addition of aggregates, the first choice will clearly give a larger result. If the overall concrete diffusivity is going up with the addition of more aggregate, the second choice will clearly give the larger value. Theoretically, it is not possible to choose between these ways of carrying out the D-EMT process, as the value of D_{ITZ} is essentially a free parameter in the problem. Ref. [51] showed how the numerically exact random walker calculations of D/D_{bulk} can show how to make a choice between these two limits.

We note that, a priori, there is no reason to expect an EMT to work well for a particular problem. The dilute limit used in the development of an EMT is exact, but the approximation used to produce predictions for larger volume fractions of aggregate are essentially uncontrolled. Having numerically exact diffusivity calculations available makes it possible to quantitatively evaluate the D-EMT predictions and optimize them for practical use. The D-EMT results can now be used to replace the random walker numerical results, but the validity of this replacement could only have been determined by having the random walker techniques available in the first place.

4.3 Discussion of multi-scale model variables

The largest difference between the multi-scale model and previous work [58,59], is the ability to take into account, even in an approximate way, the redistribution of cement due to the presence of the aggregates. This gives more accurate values of D_{ITZ} and D_{bulk}. This step appears to be crucial, especially at the high volume fractions of aggregate common in concrete, as this redistribution of cement plays an important role in determining the bulk properties of the concrete. The procedure used in the multi-scale model to determine this ratio, step (2) as given above, is still approximate, since the gradient of properties in the interfacial zone is treated as being equivalent to a fixed width, fixed property interfacial zone surrounded by fixed property bulk cement paste.

One consequence of this cement redistribution is a sort of "negative feedback" loop, in the following sense. Suppose the interfacial transition zone is made wider, by using a coarser cement, perhaps. This would tend to drive up the value of D_{ITZ}, and lower the value of D_{bulk}, so that the ratio of the two would be larger, implying a larger value of D/D_{bulk} [58]. However, the actual value of D will not be as much higher as one might predict, since the higher value of D/D_{bulk} must be multiplied by the lower value of D_{bulk} to get the overall concrete diffusivity. So just increasing the diffusivity of the interfacial zone by thickening it will not increase the overall concrete diffusivity as much as might be expected [6]. Increasing the surface area of the aggregate by reducing the average aggregate diameter results in similar behavior. Other interplays between the variables of the problem are discussed in Ref. [6], which used a statistically designed model experiment to probe which microstructural variables were significant. These were found to be: aggregate volume fraction, w/c ratio, and degree of hydration, with the thickness of the interfacial transition zone still significant but to a lesser extent.

In order to properly compare the model with experimental results, one cannot just prepare concretes at various aggregate volume fractions, and then simply normalize the concrete measurements by cement paste measurements taken at equal times. The redistribution of cement in the concrete makes the value of D_{bulk} in the concrete not the same as the plain cement paste sample, even at equal degrees of hydration. What must be done experimentally is the following. The degree of hydration of the concrete must be determined, along with the volume fraction and particle size distribution of the aggregates, and the particle size distribution of the cement, or at least its median particle size. These are the necessary microstructural variables on which the multi-scale model operates. The diffusivity or electrical conductivity of the concrete can then be measured and compared with model predictions. This procedure has been been carried out for mortars with various amounts of sand [60].

4.4 Using a sieve analysis to compute statistical quantities needed

In order to make use of the analytical parts of the multi-scale model, one must be able to compute quantities like the average radius of the aggregates, weighted according to particle *number* statistics, not particle mass statistics. Sieve analyses are commonly measured in concrete technology, and so the procedure to use the results of a sieve analysis to compute these quantites is given below.

A typical sieve analysis of an aggregate can be expressed in terms of d_i, M, and c_i, where c_i is the fraction of the total volume of aggregate that has a diameter between d_i and d_{i+1}, $d_i < d_{i+1}$, and M is the total number of sieves used. The units of the particle diameters are millimeters. The sum of c_i over the M sieves equals 1. A typical sieve analysis is expressed in terms of the mass fraction passing or retained by a certain sieve size, which can easily be converted to the form given here. If aggregates of different size all have the same density, then mass fractions are the same as volume fractions. Otherwise, conversion between mass fractions and volume fractions must be carried out.

In the ITZ volume formulas, eqs. (4)-(6), one finds powers of the aggregate radii, averaged over the number distribution density of the aggregates. The formulas below were derived to carry out this procedure using the sieve analysis. This is followed by formulas for performing volume averages, also using the sieve analysis, which are necessary to be able to evaluate the D-EMT formulas ($\langle m \rangle_V$) for a given aggregate particle size distribution.

In order to carry out these averages, an assumption is needed as to how the aggregates are distributed within each sieve. That information is not given by a sieve analysis. Many assumptions are possible, but two that are easy to handle analytically, and are physically reasonable, are that either the aggregates are distributed, within a sieve, uniformly by volume or uniformly by diameter. The analysis is shown for both assumptions, although in all previous simulation work, the former assumption was used [6,51]. The assumption could also be made, of course, that all the aggregates in a sieve have the same radius, perhaps equal to the average of the endpoints of the sieve range, but it is more accurate and realistic to assume some kind of distribution within the sieve.

4.4.1 Assumption 1: Uniform distribution by volume

In this case, the fraction of the total aggregate volume represented by particles with volumes in the range (V,V+dV), contained in the i'th sieve, is given by

$$p_i(V)\,dV = \frac{c_i dV}{(V_{i+1} - V_i)} \tag{11}$$

so that the integral over the interval (V_{i+1}, V_i) will be equal to c_i. If N is the total number of aggregate particles used per the total concrete volume V_{TOT}, so that $\rho \equiv N / V_{TOT}$, V_{agg} is the total aggregate volume, $c_{agg} = V_{agg} / V_{TOT}$, the fraction of the total *number* of aggregate particles with volumes in the range (V,V+dV), contained in the i'th sieve, is given by

$$n_i(V)\,dV = \frac{c_{agg}\, c_i\, dV}{\rho\ V\ (V_{i+1} - V_i)} \tag{12}$$

where V is the volume of a particle in this range. If we now convert to radius, using $V = 4\,\pi\, r^3 / 3$ and $dV = 4\,\pi\, r^2\, dr$, the equivalent expression in terms of the particle radius is

$$n_i(r)\,dr = \frac{9 c_{agg}\, c_i\, r^{-1} dr}{4\pi\, \rho\ \ (r_{i+1}^3 - r_i^3)} \tag{13}$$

Integrating over each sieve's endpoints and summing over each sieve must give 1 for this expression:

$$1 = \sum_{i=1}^{M} \int_{r_i}^{r_{i+1}} n_i(r)\,dr \tag{14}$$

This normalization determines the value of ρ:

$$\rho = \sum_{i=1}^{M} \frac{9 c_{agg} c_i}{4\pi\,(r_{i+1}^3 - r_i^3)} \ln\left(\frac{r_{i+1}}{r_i}\right) \tag{15}$$

Therefore, the average of R^n over the particle number density is then

$$< R^n > = \sum_{i=1}^{M} \frac{9 c_{agg} c_i}{4\pi \rho \, (r_{i+1}^3 - r_i^3)} \int_{r_i}^{r_{i+1}} r^{n-1} \, dr \tag{16}$$

Note that the quantity c_{agg} drops out of eq. (16), as it appears in the numerator and in the denominator, in ρ. This is as it should be, since $<R^n>$is the same for any representative amount of aggregate, and is independent of the total amount added to a concrete. The value of ρ does depend on c_{agg}, however, since it is the number fraction of particles in the total concrete volume.

4.4.2 Assumption 2: Uniform distribution by radius

In this case, the fraction of the aggregate volume represented by particles with radii in the range (r, r+dr), contained in the i'th sieve, is given by

$$p_i(r) dr = \frac{c_i \, dr}{(r_{i+1} - r_i)} \tag{17}$$

so that the integral of $p_i(r)dr$ over the interval (r_i, r_{i+1}) will be equal to c_i . Similar to the previous case, the fraction of the total number of aggregate particles with radii in the range (r, r+dr), contained in the i'th sieve, is given by

$$n_i(r) dr = \frac{3 c_{agg} \, c_i \, dr}{\rho \, 4\pi \, r^3 \, (r_{i+1} - r_i)} \tag{18}$$

where $V = 4 \pi r^3 / 3$ is the volume of a (spherical) particle in this range. Eq. (18) must obey the normalization (14), implying that the value of ρ is then

$$\rho = \sum_{i=1}^{M} \int_{r_i}^{r_{i+1}} \frac{3 c_{agg} c_i \, r^{-3} \, dr}{4\pi \, (r_{i+1} - r_i)} \tag{19}$$

or

$$\rho = \sum_{i=1}^{M} \frac{3 c_{agg} c_i \, (r_i + r_{i+1})}{8\pi \, (r_{i+1} r_i)^2} \tag{20}$$

Therefore, the average of R^n over the particle number density is

$$< R^n > = \sum_{i=1}^{M} \frac{3 c_{agg} c_i}{4\pi \rho \ (r_{i+1} - r_i)} \int_{r_i}^{r_{i+1}} r^{n-3} \, dr \tag{21}$$

4.4.3 Averages over the volume distribution

For averages over the volume distribution of the particles, either assumption can again be used. The starting points are the same for each assumption. Assuming a uniform distribution by volume within a sieve of the particles, the volume average $< ... >_V$ is

$$< f(r) >_V = \sum_{i=1}^{M} \frac{3 \, c_i}{(r_{i+1}^3 - r_i^3)} \int_{r_i}^{r_{i+1}} r^2 f(r) \, dr \tag{22}$$

The equation for the assumption of a uniform distribution, within a sieve, of the particles by radius, is

$$< f(r) >_V = \sum_{i=1}^{M} \frac{c_i}{(r_{i+1} - r_i)} \int_{r_i}^{r_{i+1}} f(r) \, dr \tag{23}$$

4.4.4 Example of multi-scale model calculation

To better illustrate how to use the analytical parts of the multi-scale model, an example calculation will be done that makes use of the formulas in the previous section. All data will be taken from recent work [60]. We will take a simple mortar, with an aggregate volume fraction of 50%. The sieve analysis for the aggregates is given in Table 1.

Table 1: Sieve analysis used for aggregates in mortar

Diameter Range (μm)	Fraction of Total Volume (c_i)
1180-600	0.0228
600-300	0.2193
300-150	0.749
150-75	0.0089

The overall w/c ratio is 0.4. The cement particle size distribution is such that the median diameter is 12μm, so that the ITZ is taken to have the same thickness [60]. Table 2 shows the model cement particle size distribution, taken from the real cement PSD [60].

Using the sieve analysis in Table 1, and the equations given in the previous sections, one can easily calculate the value of V_{ITZ} to be 0.0945 (using Assumption 1 and A = 0). A numerical point counting method applied to the same problem gave V_{ITZ} = 0.0918, so the analytical result differs from the numerical result by only 3%. Given that the aggregate volume fraction is 0.5, that implies that the ratio of ITZ to bulk cement paste is V_{ITZ}/V_{bulk} = 0.233, which is similar to that for Fig. 16.

Table 2: Model particle size and volume fractions for cement used

Diameter (μm)	Fraction of Cement Volume
3	0.19
5	0.082
7	0.088
9	0.065
15	0.182
25	0.193
35	0.110
45	0.09

One can then construct a 220 x 220 x 65 pixel unit cell, with a 2 pixel wide flat aggregate. The scale is one μm per pixel length, similar to that shown in Fig. 16. The ITZ region is 12 pixels thick, and the bulk region is 65 – (2) – (12) = 51 pixels long. The ratio of ITZ to bulk cement paste volume in this cell is then (220 x 220 x 12)/(220 x 220 x 51) = 0.235. One then uses the model cement PSD in Table 2 and builds up a w/c = 0.4 cement paste in the unit cell. The porosity ratio, and therefore the diffusivity ratio, are determined as a function of degree of hydration.

4.4.5 Effect of hydration on the value of D_{ITZ}/D_{bulk}

An interesting prediction of the multi-scale diffusivity model is that the contrast in diffusivity, D_{ITZ}/D_{bulk}, between the ITZ and the bulk cement paste, changes with hydration. This is easily seen for a homogeneous C_3S cement paste, for which the capillary porosity ϕ as a function of degree of hydration α is given by the straight line [8]:

$$\phi = 1 - \frac{1 + 1.13\alpha}{1 + 3.21 w/c} \tag{24}$$

The value 3.21 is the specific gravity of C_3S, and the value 1.13 comes from the volumes of various hydration products allowing for chemical shrinkage and fully saturated curing conditions [8]. For different values of w/c, the slope of the line is different. For the system considered, the porosity in the ITZ and the bulk regions was found to decrease linearly with degree of hydration. Since the cement paste diffusivity depends non-linearly on porosity, that means that the diffusivity ratio between bulk and ITZ paste will change with hydration. Figure 17 shows the results for D_{ITZ}/D_{bulk} for this system as a function of degree of hydration. The points are from recent experimental results [60], obtained by applying the D-EMT to the experimental measurements. There is qualitative agreement between experiment and the multi-scale model predictions. The degree of hydration at which the maximum value of D_{ITZ}/D_{bulk} is obtained is about 0.6 for experiment, and 0.7 for the multi-scale model. Also, the experimental points, except at late hydration, are well above the model points. This implies that the model needs improvement for handling how much hydration product forms in the ITZ, in order to make the porosity difference greater. One should also note that the experimental points were obtained by applying D-EMT to experimental data, and extracting the effective value of D_{ITZ}/D_{bulk}, so that there is probably some systematic error in the experimental points. Notice that at later hydration, the agreement becomes closer, implying that the multi-scale model gives more quantitative predictions for later hydration times. For durability considerations, it may only be necessary to give accurate diffusivity predictions at later hydration times.

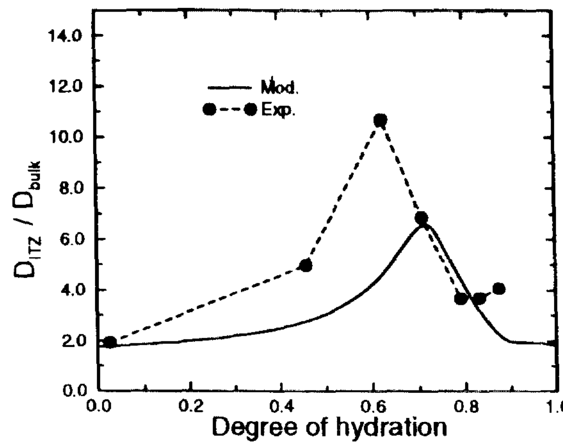

Figure 17: Plot of the value of D_{ITZ}/D_{bulk} vs. degree of hydration for the example mortar discussed in the text.

5. Summary and Research Needs

This chapter has shown how the microstructure around a single aggregate, as influenced by aggregate properties, cement size, and the presence of mineral admixtures, can be quantitatively modelled using mainly micrometer-scale digital-image-based models, in order to be able to handle the random microstructural changes that occur during hydration. The geometry and topology of the many ITZ regions that occur in a real material have been studied using millimeter-scale continuum models. These models can handle some of the effect of aggregate shape, and can quantitatively explore the interconnectedness of the ITZ regions. The effect on the ionic diffusivity or electrical conductivity of a mortar or concrete of ITZ geometry and properties can be studied in a multi-scale approach, with reasonable agreement with available experimental evidence.

Work to be done includes obtaining more experimental measurements of concrete diffusivity and conductivity, along with degrees of hydration, and aggregate and cement particle size distributions, to better compare with the multi-scale model predictions. The multi-scale model probably needs to be improved in its use of effective medium theory, the formula used for cement paste diffusivity as a function of porosity, and the distribution of hydration products between bulk and interfacial transition zone cement paste. Also, the effect of mineral admixtures on ITZ and bulk microstructure and transport properties must be quantified and added to the multi-scale model. Further work in these areas is on-going.

6. References

1. Maso, J.C., "The Bond Between Aggregates and Hydrated Cement Pastes," Proc. 7th Inter. Congress on the Chemistry of Cement, 3-15 (1980).
2. Bentz, D.P., Schlangen, E., and Garboczi, E.J., "Computer Simulation of Interfacial Zone Microstructure and Its Effect on the Properties of Cement-Based Composites," in *Materials Science of Concrete IV*, ed. by J.P. Skalny and S. Mindess (American Ceramic Society, Westerville, OH, 1995) 155-200.
3. Ollivier, J.P., Maso, J.C., and Bourdette, B., "Interfacial Transition Zone in Concrete," Adv. Cem.-Based Mater. **2**, 30-38 (1995).
4. Bentz, D.P., Hwang, J.T.G., Hagwood, C., Garboczi, E.J., Snyder, K.A., Buenfeld, N., and Scrivener, K.L., "Interfacial Zone Percolation in Concrete: Effects of Interfacial Zone Thickness and Aggregate Shape," in *Microstructure of Cement-Based Systems/Bonding and Interfaces in Cementitious Materials* **370** (Materials Research Society, Pittsburgh, 1995), 437-442.
5. Perram, J.W., and Wertheim, M.S., "Statistical Mechanics of Hard Ellipsoids. I. Overlap Algorithm and the Contact Function," J. Comput. Phys. **58**, 409-416 (1985).
6. Bentz, D.P., Garboczi, E.J., and Lagergren, E.S., "Multi-scale microstructural modelling of concrete diffusivity: Identification of significant variables," ASTM

Cem. Conc. & Agg. **20**, 129-139 (1998). Available at: http://ciks.cbt.nist.gov/garboczi/, Chapter 7 Section 3.

7. Bentz, D.P., "A Three-Dimensional Cement Hydration and Microstructure Program. I. Hydration Rate, Heat of Hydration, and Chemical Shrinkage," NISTIR **5756**, U.S. Department of Commerce, November 1995.
8. Bentz, D.P., "Three-Dimensional Computer Simulation of Cement Hydration and Microstructure Development," J. Amer. Ceram. Soc. **80**, 3-21 (1997). Newest version of hydration code manual available at http://ciks.cbt.nist.gov/garboczi/, Appendix 2.
9. Hashin, Z., "Analysis of Composite Materials: A Survey," J. Applied Mech. **50**, 481-505 (1983).
10. Torquato, S., "Random heterogeneous media: Microstructure and improved bounds on effective properties," Appl. Mech. Rev. **44**, 37-76 (1991).
11. Garboczi, E.J., and Bentz, D.P., "Multi-Scale Picture of Concrete and Its Transport Properties: Introduction for Non-Cement Researchers," NISTIR **5900**, U.S. Department of Commerce, October 1996. Also available at http://ciks.cbt.nist.gov/garboczi/, Appendix 1.
12. van Breugel, K., "Simulation of Hydration and Formation of Structure in Hardening Cement-Based Materials," Ph. D. Thesis, Delft University of Technology, The Netherlands, 1991.
13. Bentz, D.P., Garboczi, E.J., and Stutzman, P.E., "Computer Modelling of the Interfacial Zone in Concrete," in *Interfaces in Cementitious Composites*, ed. J.C. Maso (E&FN Spon, London, 1992) pp. 107-116. Also available at: http://ciks.cbt.nist.gov/garboczi/, Chapter 6, Section 3.
14. Garboczi, E.J., and Bentz, D.P., "Digital Simulation of the Aggregate-Cement Paste Interfacial Zone in Concrete," J. Mater. Res. **6**, 196-201 (1991).
15. Grutzek, M.W., Shi, D., Liu, G., and Kwan, S., "Computer Simulation of Interfacial Packing in Concrete," J. Mater. Sci. **28**, 3444-3450 (1993).
16. Scrivener, K.L., and Pratt, P.L., "Characterization of Interfacial Microstructure," in *Interfacial Transition Zone in Concrete*, ed. J.C. Maso (E & FN Spon, London, 1996) 3-17.
17. Breton, D., Carles-Gibergues, A., Ballivy, G., and Grandet, J., "Contribution to the Formation Mechanism of the Transition Zone Between Rock-Cement Paste," Cem. Conc. Res. **23**, 335-346 (1993).
18. Monteiro, P.J.M., Gjorv, O.E., and Mehta, P.K., "Microstructure of the Steel-Cement Paste Interface in the Presence of Chlorides," Cem. Conc. Res. **15**, 781-784 (1985).
19. Zayed, A.M., "The Nature of the Concrete-Steel Rebar Interface in Plain and Silica Fume Concrete," in *Advanced Cementitious Systems: Mechanisms and Properties* (Materials Research Society, Pittsburgh, PA, 1992) 341-347.
20. Yuan, C.Z. and Odler, I., "The Interfacial Zone Between Marble and Tricalcium Silicate Paste," Cem. Conc. Res. **17**, 784-792 (1987).

21. Larbi, J.A. and Bijen, J.M.J.M., "Effects of Water-Cement Ratio, Quantity and Fineness of Sand on the Evolution of Lime in Set Portland Cement Systems," Cem. Conc. Res. **20**, 783-794 (1990).
22. Saito, M. and Kawamura, M., "Effect of Fly Ash and Slag on the Interfacial Zone Between Cement and Aggregate," in *Fly Ash, Silica Fume, and Natural Pozzolans in Concrete*, ACI SP-114, edited by V.M. Malhotra (ACI, Detroit, 1989) 669-688.
23. Bentz, D.P., Garboczi, E.J., and Stutzman, P.E., "Experimental and Simulation Studies of the Interfacial Zone in Concrete," Cem. Conc. Res. **22**, 891-902 (1992).
24. Bentz, D.P. and Garboczi, E.J., "Simulation Studies of the Effects of Mineral Admixtures on the Cement Paste-Aggregate Interfacial Zone," ACI Mater. J. **88**, 518-529 (1991).
25. Berry, E.E., Hemmings, R.T., Langley, W.S., and Carrette, G.G., "Beneficiated Fly Ash: Hydration, Microstructure, and Strength Development in Portland Cement Systems," *in Fly Ash, Silica Fume, and Natural Pozzolans in Concrete*, ACI SP-114, edited by V.M. Malhotra (ACI, Detroit, 1989) 241-273.
26. Sybertz, F., "Comparison of Different Methods for Testing the Pozzolanic Activity of Fly Ashes," in *Fly Ash, Silica Fume, and Natural Pozzolans in Concrete*, ACI SP-114, edited by V.M. Malhotra (ACI, Detroit, 1989) 477-497.
27. Slanicka, S. and Lamacska, S., "The Influence of Fly Ash Fineness on the Strength of Concrete," Cem. Conc. Res. **21**, 285-296 (1991).
28. Cornelissen, H.A.W. and Gast, C.H., "Upgrading of PFA for Utilization in Concrete," in *Fly Ash, Silica Fume, and Natural Pozzolans* in Concrete, ACI SP-131, edited by V.M. Malhotra (ACI, Detroit, 1992) 457-470.
29. Zhang, M.H., Lastra, R., and Malhotra, V.M., "Rice-Husk Ash Paste and Concrete: Some Aspects of Hydration and the Microstructure of the Interfacial Zone Between the Aggregate and Paste," Cem. Conc. Res. **26**, 963-977 (1996).
30. Ollivier, J.P. and Massat, M., "Microstructure of the Paste-Aggregate Interface, Including the Influence of Mineral Additions," in *Advances in Cement and Concrete* (Engineering Foundation, New York, 1994), 175-185.
31. Scrivener, K.L., Bentur, A., and Pratt, P.L., "Quantitative Characterization of the Transition Zone in High Strength Concretes," Adv. Cem. Res. **1**, 230-237 (1988).
32. Bentur, A. and Cohen, M.D., "Effect of Condensed Silica Fume on the Microstructure of the Interfacial Zone in Portland Cement Mortars," J. Amer. Ceram.Soc. **70**, 738-743 (1987).
33. Monteiro, P.J.M., Gjorv, O.E., and Mehta, P.K., "Effect of Condensed Silica Fume on the Steel-Cement Paste Transition Zone," Cem. Conc. Res. **19**, 114-123 (1989).
34. Lagerblad, B. and Utkin, P., "Silica Granulates in Concrete- Dispersion and Durability Aspects," CBI Report 3:93 (Swedish Cement and Concrete Research Institute, Stockholm, 1993).
35. Zhang, M.H. and Gjorv, O.E., "Microstructure of the Interfacial Zone Between Lightweight Aggregate and Cement Paste," Cem. Conc. Res. **20**, 610-618 (1990).
36. Holm, T.A., Bremner, T.W., and Newman, J.B., "Lightweight Aggregate Concrete Subject to Severe Weathering," Conc. Inter. **6**, 49-54 (June, 1984).

37. Fagerlund, G., "Frost Resistance of Concrete with Porous Aggregate," Report of the Cement and Concrete Institute in Sweden (1978).
38. Berger, R.L., "Properties of Concrete with Cement Clinker Aggregate," Cem. Conc. Res. **4**, 99-112 (1974).
39. Zimbelmann, R., "A Method for Strengthening the Bond Between Cement Stone and Aggregates," Cem. Conc. Res. **17**, 651-660 (1987).
40. Yang, S., Zhongzi, X., Ping, X., and Mingshu, T., "A New Method of Enhancing Cement-Aggregate Interfaces I. Ideal Aggregate and Its Effect on Interfacial Microstructures," Cem. Conc. Res. **22**, 612-618 (1992).
41. Yang, S., Zhongzi, X., Ping, X., and Mingshu, T., "A New Method of Enhancing Cement-Aggregate Interfaces II. Mechanical Properties and Sulphate Attack Resistances of Mortars," Cem. Conc. Res. **22**, 769-773, 1992.
42. Mitsui, K., Li, Z., Lange, D.A., and Shah, S.P., "A Study of Properties of the Paste-Aggregate Interface," in *Interfaces in Cementitious Composites*, edited by J.C. Maso (E & FN Spon, London, 1992) 119-128.
43. Desai, P.G., Xu, Z., and Lewis, J.A., "Synthesis and Properties of $CaAl_2O_4$-Coated Al_2O_3 Microcomposite Powders," J. Amer. Ceram. Soc. **78**, 2881-2888 (1995).
44. Feldman, R.F., "The Effect of Sand/Cement Ratio and Silica Fume on the Microstructure of Mortars," Cem. Conc. Res. **16**, 31-39 (1986).
45. Winslow, D.N. and Lui, D., "The Pore Structure of Paste in Concrete," Cem. Conc. Res. **20**, 227-235 (1990).
46. Scrivener, K.L. and Nemati, K.M., "The Percolation of Pore Space in the Cement Paste/Aggregate Interfacial Zone of Concrete," Cem. Conc. Res. **26**, 35-40 (1996).
47. Torquato, S., "Bulk Properties of Two-Phase Disordered Media, 1. Cluster Expansion for the Dielectric Constant of Dispersions of Penetrable Spheres," J. Chem. Phys. **81**, 5079-5088 (1984).
48. Winslow, D.N., Cohen, M.D., Bentz, D.P., Snyder, K.A., and Garboczi, E.J., "Percolation and Pore Structure in Mortars and Concrete," Cem. Conc. Res. **24**, 25-37 (1994).
49. Bourdette, B., Ringot, E., and Ollivier, J.P., "Modelling of the Transition Zone Porosity," Cem. Conc. Res., **25**, 741-751 (1995).
50. Johansen, V. and Thaulow, N., "At What Scale do Homogeneous Phenomena Become Localized: The Necessary and Sufficient Magnification," in *The Modelling of Microstructure and Its Potential for Studying Transport Properties and Durability*, edited by H.M. Jennings et al. (Kluwer Academic Publishers, The Netherlands, 1996) 65-89.
51. Garboczi, E.J. and Bentz, D.P., "Multi-scale analytical/numerical theory of the diffusivity of concrete," Advanced Cement-Based Materials **8**, 77-88 (1998). Also available at http://ciks.cbt.nist.gov/garboczi/, Chapter 7, Section 4.
52. Diamond, S., Mindess, S., and Lovell, J., "On the Spacing Between Aggregate Grains in Concrete and the Dimension of the Aureole de Transition," *in Liaisons Pates de Ciment Materiaux Associes* (RILEM, Toulouse, France, 1982) C42.
53. Lu, B., and Torquato, S., Phys. Rev. A **45**, 5530-5544 (1992).

54. E.J. Garboczi and D.P. Bentz, Adv. Cem.-Based Mater. **6**, 99-108 (1997). Also available at: http://ciks.cbt.nist.gov/garboczi/, Chapter 7, Section 8.
55. E.J. Garboczi, K.A. Snyder, J.F. Douglas, and M.F. Thorpe, Phys. Rev. E **52**, 819-828 (1995). Also available at: http://ciks.cbt.nist.gov/garboczi/, Ch. 3, Section 2.
56. Bentz, D.P., Quenard, D.A., Baroghel-Bouny, V., Garboczi, E.J., and Jennings, H.M., Mater. and Struc. **28**, 450-58 (1995).
57. Bentz, D.P., Detwiler, R.J., Garboczi, E.J., Halamickova, P., and Schwartz, L.M., "Multi-Scale Modelling of the Diffusivity of Mortar and Concrete," RILEM International Conference on Chloride Intrusion into Concrete, 1995.
58. Garboczi, E.J., Schwartz, L.M., and Bentz, D.P., Adv. Cem.-Based Mater. **2**, 169-181 (1995).
59. Schwartz, L.M., Garboczi, E.J.,and Bentz, D.P., J. Appl. Phys. **78**, 5898-5908 (1995).
60. Shane, J., Mason, T.O., Bentz, D.P., Garboczi, E.J., and Jennings, H.M., in preparation (1998).
61. Rashed, A.I., and Williamson, R.B., Journal of Materials Research **6**, 2004-2012 (1991).
62. Snyder, K.A., and Clifton, J.R., "Measures of Air Void Spacing," in *Proceedings of International Conference on Building Materials: Volume 1*, Weimar, Germany, 155-158, 1994.
63. Scrivener, K.L., "Microstructure of Concrete," in *Materials Science of Concrete Vol. I*, edited by J. Skalny (American Ceramic Society, Westerville, Ohio, 1989), pp. 127-161.
64. Garboczi, E.J., and Bentz, D.P., Journal of Materials Science **27**, 2083-2092, 1992.
65. Christensen, B.J., Mason, T.O., Jennings, H.M., Bentz, D.P., and Garboczi, E.J.,in *Advanced Cementitious Systems: Mechanisms and Properties Vol. 245*, edited by F.P. Glasser, G.J. McCarthy, J.F. Young, T.O. Mason, and P.L. Pratt (Materials Research Society, Pittsburgh, 1992), pp. 259-264. Also available at http://ciks.cbt.nist.gov/garboczi/, Chapter 5, Section 3.
66. Garboczi, E.J. and Bentz, D.P., "The effect of the interfacial zone on concrete properties: The dilute limit," in *Materials for the New Millenium*, edited by K.P. Chong (ASCE, New York, 1996), pp. 1228-1237. Also available at: http://ciks.cbt.nist.gov/garboczi/, Chapter 7, Section 7.
67. Mills, R., and Lobo, V.M.M., *Self-Diffusion in Electrolyte Solutions* (Elsevier, Amsterdam, 1989) p. 317.
68. Cooper, D.W., Phys. Rev. A **38**, 522-524 (1988).
69. McLaughlin, R., Int. J. Eng. Sci. **15**, 237-244 (1977).